

UNCLASSIFIED
CONFIDENTIAL

Copy 5
RM E56G25

c.1

NACA RM E56G25

NACA

RESEARCH MEMORANDUM

EXPERIMENTAL INVESTIGATION OF A HIGH SUBSONIC MACH NUMBER
TURBINE HAVING LOW ROTOR SUCTION-SURFACE DIFFUSION

By *W. H. Hauser* and *W. J. Nusbaum*

Lewis Flight Propulsion Laboratory
Cleveland, Ohio

LIBRARY COPY

OCT 15 1956

LANGLEY AERONAUTICAL LABORATOR
LIBRARY, NACA
LANGLEY FIELD, VIRGINIA

CLASSIFIED DOCUMENT

This material contains information affecting the National Defense of the United States within the meaning of the espionage laws, TITLE 18, U.S.C., Secs. 793 and 794, the transmission or revelation of which in any manner to an unauthorized person is prohibited by law.

**NATIONAL ADVISORY COMMITTEE
FOR AERONAUTICS**

WASHINGTON

October 10, 1956

CONFIDENTIAL

UNCLASSIFIED

CLASSIFICATION CHANGED
UNCLASSIFIED

Authority of *TPA 839* Date *1/2/67*

UNCLASSIFIED

NASA Technical Library



3 1176 01436 1142

NACA RM E56G25

NATIONAL ADVISORY COMMITTEE FOR AERONAUTICS

RESEARCH MEMORANDUM

EXPERIMENTAL INVESTIGATION OF A HIGH SUBSONIC MACH NUMBER TURBINE

HAVING LOW ROTOR SUCTION-SURFACE DIFFUSION

By Cavour H. Hauser and William J. Nusbaum

SUMMARY

As part of a program to establish limits for the aerodynamic design parameters of the turbine component for advanced supersonic aircraft, a number of experimental turbines are currently being investigated. The cold-air turbine investigated herein was designed for a high weight flow per unit frontal area, a high specific work output, and a rotor hub inlet relative critical velocity ratio of 0.82.

The performance of the turbine was determined over a range of operating conditions. At the equivalent design blade speed and work output, the brake internal efficiency based on the actual total-pressure ratio was 0.875, which is almost as high as those obtained in conservatively designed turbines. In running the turbine at the point of limiting blade loading for the rotor and equivalent design blade speed, the efficiency dropped 0.05 from that obtained at the design point. This increase in loss was apparently caused by the shock waves and attendant boundary-layer losses on the portion of the rotor blade suction surface downstream of the channel exit. The calculated ratio of effective rotor blade momentum thickness to mean camber length of 0.0104 at the design operating point agrees reasonably well with the results of previous work on other turbines.

INTRODUCTION

The turbine component suitable for use in the power plant of an advanced supersonic aircraft should have a high specific work output per stage and high mass flow per unit frontal area. These requirements necessitate the use of high relative Mach numbers at the rotor entrance and low hub-tip radius ratios without a sizeable reduction in turbine efficiency from that obtainable with more conservative designs.

As part of a program to establish values of design parameters that will result in high efficiencies in turbines for the previously described

UNCLASSIFIED

CW-1

application, a number of experimental turbine design configurations have been and are currently being investigated at the NACA Lewis Laboratory. In reference 1, for example, a turbine designed for conservative velocities through the blade rows is shown to have a design-point efficiency of 0.89. This turbine was designed for a hub-tip radius ratio of 0.60, giving a relatively high value of weight flow per unit frontal area. The rotor hub inlet critical velocity ratio was only 0.6, however, thus limiting the work output to relatively low values.

Efficiencies as high as 0.87 may be obtained in turbines designed for much higher velocity levels, as shown in references 2 to 4. These turbines were designed for a rotor hub inlet relative critical velocity ratio of 1.0 and a hub-tip radius ratio of 0.70. Thus, while the work output of this turbine is considerably higher than the conservatively designed turbine of reference 1, the efficiency is slightly lower and the weight-flow capacity is reduced.

In consideration of these results it was believed that high efficiency could be obtained in a single-stage turbine with a rotor hub inlet relative critical velocity ratio of about 0.8. This increase in inlet relative critical velocity ratio over that in reference 1 results in an increase in specific work output for a given rotative speed. If a hub-tip radius ratio of 0.60 is used, the weight flow per unit frontal area is about the same as that for the turbine of reference 1. Thus, with a high weight flow per unit frontal area and a high efficiency at high specific work output, the proposed turbine should be particularly well suited for use in the power plant of an advanced supersonic aircraft.

The present investigation presents the aerodynamic blade design method and the performance characteristics of the first of a series of turbines designed according to the previously stated specifications.

In the present rotor blade design, the diffusion of the suction-surface velocity is held to comparatively conservative limits. The suction-surface diffusion parameter is held to zero at the hub and is small at other radii. In the design of the rotor blade passage, radial equilibrium of the flow was maintained by assuming a free-vortex condition along radial elements through the mean streamlines. The quasi-three-dimensional design procedure used for the stator blades is presented herein.

The turbine performance was obtained over a range of speed from 60 to 110 percent of design rotative speed and actual total-pressure ratios from 1.3 to the limiting-loading condition (about 2.2). The inlet temperature and pressure were nominally 80° F and 24.6 pounds per square inch absolute, respectively.

TURBINE DESIGN

Requirements

It was desired to design a turbine having high weight flow per unit frontal area and high work output while at the same time maintaining good aerodynamic blading efficiency.

The cold-air turbine used in this investigation is 14 inches in diameter and has a constant hub-tip radius ratio of 0.60. The over-all design requirements, which were chosen for application of the turbine in the power plant of an advanced supersonic aircraft, are as follows:

| | |
|---|-------|
| Equivalent specific work output, $\Delta h' / \omega_{cr}$, Btu/lb | 20.60 |
| Equivalent weight flow, $w \sqrt{\omega_{cr}} / \delta$, lb/sec | 16.10 |
| Equivalent blade tip speed, $U_t / \sqrt{\omega_{cr}}$, ft/sec | 720 |

(All symbols are defined in appendix A.)

Velocity Diagrams

The design velocity diagrams at the free-stream stations 1, 3, and 5 were determined on the basis of the following assumptions:

- (1) Free-vortex flow
- (2) Simplified radial equilibrium
- (3) Stator over-all total-pressure ratio p_3^*/p_1^* of 0.98
- (4) Over-all adiabatic efficiency design value of 0.90

These velocity diagrams together with those calculated for stations 2 and 4 (just upstream of the blade trailing edge in the stator and rotor, respectively) are presented in figure 1.

These diagrams show that, because of the relatively low radius ratio (0.60) and because of the free-vortex design, a rather wide variation occurs in the flow conditions from hub to tip in both the stator and rotor. For example, the critical velocity ratio V/a_{cr}^* at the stator exit (station 3) varies from a supersonic value (1.146) at the hub to 0.775 at the tip section. The air-turning angle through the rotor $\beta_3 - \beta_5$ varies from 95° at the hub to 41.2° at the tip section. The relative inlet-air angle β_3 varies from 54.8° at the hub to -9.4° at the tip. Thus, there is considerable twist required in the rotor blade from hub to tip sections.

At the hub of the rotor, the relative inlet critical velocity ratio $(W/a_{cr}'')_3$ is 0.824, and the free-stream value at the exit $(W/a_{cr}'')_5$ is 0.888, indicating a slight positive reaction across the rotor (fig. 1(a)).

The energy loss caused by the whirl component of the absolute velocity at the rotor exit (station 5), mass-averaged over the blade height, amounts to 0.8 percent of the design work output.

Velocity diagrams at stations 2 and 4, just upstream of the stator and rotor blade trailing edges, respectively, were calculated in a manner similar to that described in reference 2. Between stations 2 and 3 in the stator and also between stations 4 and 5 in the rotor it was assumed that no change occurred in the tangential velocity component. A stator-outlet to -inlet total-pressure ratio p_2^t/p_1^t of 0.99 was assumed, and zero pressure loss was assumed between stations 4 and 5 in the rotor. Thus, the velocity diagrams at stations 2 and 4 can be determined on the basis of continuity and trailing-edge blockage factors, which can be calculated from the number of blades, the flow angle downstream of the trailing edge, and the trailing-edge thickness for each blade row.

The relative velocities at the rotor exit (station 4) approach the limiting-loading condition quite closely. The maximum attainable relative tangential velocity component W_u/a_{cr}'' for a blade with a straight suction surface downstream of the throat and with a given exit flow angle (measured from the tangential direction) is given in figure 3 of reference 5. Although the rotor blades were designed with some curvature downstream of the throat, a close approximation of the limiting-loading condition is obtained by using the relative flow angle β_4 in reading this figure. This process indicates that at the design condition the tip section of the rotor blade is at the limiting-loading condition, while the mean and hub sections approach this condition closely. Also, the relatively high blockage causes the rotor to be choked at station 4, with critical velocity ratios ranging from 0.996 at the hub to 1.094 at the tip section (figs. 1(a) and (c), respectively).

Stator Blade Design

In the design of stator blades, obtaining minimum blade viscous losses is desired. For a given blade height, this can be accomplished by optimizing the solidity and the number of blades using the procedure of reference 6 as outlined in the next section.

It was assumed that simplified radial equilibrium exists along radial elements at each axial station through the blade passage. The total-pressure drop between stations 1 and 2 is assumed to occur linearly in the axial direction.

Procedure. - In general, the three-dimensional blade design procedure of references 2 and 7 was used in designing the stator blades. The design procedure is outlined herein, however, because there are some differences between the method used for the subject stator blades and those of the references:

(1) The solidity at the mean blade section was selected using the criteria of reference 8 which are shown by reference 6 to give values close to the optimum solidity. As shown in reference 6, the effect of varying the number of blades on the blade viscous loss is almost negligible in the range of the optimum number of blades; therefore, considering the trailing-edge blockage required, the number of blades was selected to be slightly less than the optimum number indicated in the reference. The axial chord at the mean blade section was then estimated from the solidity and an estimated value of the blade-chord angle γ° .

(2) In an attempt to obtain constant blade loading from the hub to the tip blade sections, the axial chords at the hub, mean, and tip radial stations were calculated by the method presented in appendix B.

(3) A blade shape was first approximated as follows:

(a) For the hub, mean, and tip radial stations, a straight suction surface was drawn from the throat to the trailing edge at angles $\alpha_{2,h}$, $\alpha_{2,m}$, and $\alpha_{2,t}$, respectively. The procedure for calculating these angles is presented in appendix C.

(b) The first approximate profiles were then laid out so that the larger portion of the turning takes place near the blade leading edges where the flow has low momentum. Positions of velocity potential lines and midchannel streamlines were estimated.

(4) At each section a suction-surface velocity equal to the blade-outlet velocity was assumed along the entire length of the suction surface, and the pressure-surface velocity distributions were then calculated by the simplified stream-filament method found in reference 9.

(5) By using the velocity distribution of step (4), the circulation around each section was calculated by numerical integration of the line integral of the surface velocity around the blade. The blade suction surface was then modified until the circulation satisfied the relation

$$\Gamma = s(V_{u,1} - V_{u,2}) \quad (1)$$

(6) The midchannel streamline velocity distribution at the hub was adjusted to give a smooth variation in velocity from the entrance to the exit of the channel. This velocity distribution was then used to recalculate surface velocities.

(7) The surface velocities obtained in step (6) were used to recalculate and check the circulation around the hub section as in step (5). A check was also made to see that the value of the diffusion parameter on the suction surface D_s did not exceed an assigned value of 0.25.

(8) Velocity potential lines were relocated in order to satisfy irrotationality of the flow. The position of the mean streamline was calculated so that equal amounts of gas would pass on either side as discussed in appendix B of reference 9.

(9) By using the method given in appendix B of reference 7 and the mean-streamline velocity distribution at the hub from step (6), the blade shape was analyzed to obtain the mean-streamline velocity distribution at the mean and tip sections that must exist in order to satisfy simplified-radial-equilibrium conditions.

(10) The mean-streamline velocity distributions obtained in step (9) were then used to recompute the surface velocities at the mean and tip sections.

(11) With the surface velocities determined at the three blade sections, the weight flow was calculated at each axial station using the method given in appendix B of reference 7.

(12) If the results of step (11) indicated that the blade would not pass the design weight flow, then either the blade shape was changed or a different velocity distribution was assumed at the hub section. Steps (6) to (11) were then repeated.

(13) Steps (7) and (8), which apply to the hub section, were repeated for the mean and tip sections.

(14) Finally, using the calculated mean streamline positions at the mean and tip sections, steps (9) to (12) were repeated until a final satisfactory blade was evolved.

The resulting stator blade-section profiles obtained in these steps are shown in figure 2. The coordinates of each of these blade sections are given in table I(a). Figure 3 is a photograph of half the stator casing with the blades in place.

In order to obtain the final blade shape, the stator blade profiles for the hub, mean, and tip sections were stacked so that the midpoints of the potential lines across the channel exits at the three sections were on a radial line.

5008

The blade sections as designed with the previously described method actually described the profiles of the cylindrical cross sections of the blade. The method used for obtaining coordinates for flat templates from the design blade sections is discussed in appendix C of reference 7.

Discussion. - As stated previously and as shown in figure 2, the axial chord of the stator varies considerably from hub to tip, the chord at the hub being only about one-third of that at the tip. Thirty stator blades were used having values of solidity of 1.3, 1.5, and 1.6 for the hub, mean, and tip sections, respectively. In an attempt to obtain constant blade loading over the blade height, the method of appendix B holds constant the degree to which the design blade loading at each radial station approaches an "ideal" blade loading for which the exit static pressure is effective over the entire blade suction surface while the inlet total pressure is effective over the pressure surface.

The design velocity distributions on the mean streamline and the blade surfaces at the hub, mean, and tip sections are shown in figure 4. If the areas enclosed by the velocity-distribution curves on the suction and pressure surfaces at each of the three radial stations were similar in shape, the pressure- and suction-surface diffusion parameters would be nearly equal at the three stations. However, the final velocity distributions obtained do not satisfy this criterion. The velocity on the pressure surface is less than the inlet value for about 60 percent of the surface length at the tip section, whereas the flow accelerates from the leading edge at the hub. As a result, the diffusion on the suction surfaces increases markedly from the tip to the hub section in order to obtain the required turning of the flow for the chosen solidity at each radius. The suction-surface diffusion parameters at the hub, mean, and tip sections are 0.26, 0.18, and 0.10, respectively (table II). These values are considered satisfactory. In order to obtain more nearly constant diffusion over the blade height, however, there should be less radial taper in the chord length from the tip to the hub sections.

Rotor Blade Design

Procedure. - A three-dimensional design procedure was used in obtaining the rotor blade profiles. The total-pressure drop between stations 3 and 4 was assumed to be linear in the axial direction. The general procedure used in designing the two-dimensional blade profiles at each radial station is that given in reference 10. The method requires boundary conditions consisting of one streamline with the velocity distribution on that streamline. The blade passage surfaces are then derived through a step-by-step calculation process for obtaining an arbitrary number of stream filaments, each carrying a specified portion of the total mass flow. The channel boundary (blade surfaces) is the final two outermost streamlines, which will carry the total blade passage mass flow.

The rotor blade design procedure is given in the following steps:

(1) The blade chord at the mean section was chosen arbitrarily. The number of blades was then determined by applying the criterion of reference 8 (using a coefficient of aerodynamic loading of 0.80) at the blade mean section.

(2) The weight-flow function $f(w)$ was computed for the hub, mean, and tip sections from the velocity diagram calculations of stations 3 and 4. At each radius, a linear variation in this function was assumed in the axial direction between these stations.

(3) At the hub station a suction surface was arbitrarily assigned to give the required total turning. About 8° of turning was assumed both upstream and downstream of the guided channel. The velocity distribution was then assigned on this surface to give zero diffusion.

(4) The coordinates and the velocity distribution for the pressure surface of the blade hub section were determined by applying the method of reference 10 in a series of four steps across the guided-channel portion of the blade. The method used assumes a vortex-type variation of streamline curvature along the equipotential lines. The curvatures of the streamlines were determined by using the curvometer described in appendix B of reference 4.

(5) The two surfaces of the channel designed in steps (3) and (4) were faired to leading- and trailing-edge circles having radii of 0.010 and 0.015 inch, respectively.

(6) The velocities on the blade surfaces were also computed using the direct stream-filament method of reference 9.

(7) The circulation Γ around the blade was determined from a graphical integration of the velocities calculated in step (6). The value obtained was compared with that computed by the relation

$$\Gamma = s(W_{u,3} - W_{u,4}) \quad (2)$$

The suction surface of the blade was then modified and steps (4) to (6) repeated until equation (2) and the condition of zero suction-surface diffusion were satisfied.

(8) Using the mean streamline at the hub station and the calculated velocity on this streamline, the shape of the blade profiles and the velocity distribution for the mean streamlines at the mean and tip radial stations were calculated using the free-vortex relations along radial elements. The method used is presented in appendix D.

(9) The procedure followed in steps (3) to (7) in designing the hub blade section was essentially repeated for the design of the blade mean and tip sections. The blade shapes were obtained by constructing the new streamlines in both directions from the mean streamlines calculated in step (8).

(10) Finally, at each axial station through the guided passage and in planes perpendicular to the turbine axis, the total weight flow was integrated by the equation

$$w = n_R \int_{r_h}^{r_t} \int_0^{l_0} \rho W \, dl \, dr \quad (3)$$

In this calculation a linear variation in static pressure was assumed to exist across the passage in a tangential direction from the suction to the pressure surfaces at each station. This method of calculating the weight flow is the same as that described in reference 3. Where the error in the integrated weight flow was found to be greater than 1 percent of the design value at any station, alteration of the profiles was required.

The resulting blade-section profiles obtained from these steps are shown in figure 2, and the coordinates are given in table I(b). A photograph of the rotor is shown in figure 5.

In order to obtain the final blade shape, the profiles for the hub, mean, and tip sections were stacked so that the trailing edge of each section was tangent to a radial plane and the centroid of each section lay in a common radial-axial plane.

Discussion. - Fifty-eight blades were used in the rotor. The design mean-streamline and blade surface velocity distributions for the hub, mean, and tip sections of the rotor blade are shown in figure 6. The design requirement of low suction-surface diffusion has been well satisfied with diffusion parameters D_s equal to 0, 0.06, and 0.12 at the hub, mean, and tip sections, respectively (table II). In order to obtain the required over-all blade loading with these low suction-surface diffusion parameters, slightly larger values of diffusion on the blade pressure surface are required. The pressure-surface diffusion parameters D_p are 0.27, 0.12, and 0.06 at the hub, mean, and tip sections of the rotor blade, respectively (table II). These values are conservative as compared with some of the values for the transonic turbines presented in figure 9 of reference 4.

In the blade design method used, it is difficult to assign specific values for the blade surface diffusion parameters over the blade height. Once the blade profile and the velocity distribution at the hub section

have been calculated, the blade profiles and velocities at the mean and tip sections can be determined. However, experience has shown that for reasonably assigned boundary conditions the method gives satisfactory blade profiles and diffusion parameters after several trial calculations.

APPARATUS AND PROCEDURE

The experimental equipment used in the present investigation is basically the same as that described in reference 1. Figure 2 of reference 1 is a photograph of the turbine installation with the upper half of the casing removed. A schematic cross section of the installation showing the various instrumentation stations used herein is presented in figure 7. The stator blades were machined from mild steel, the rotor blades from aluminum alloy, and all were hand-finished. The radial tip clearance of the rotor was 0.030 inch.

Instrumentation

The total conditions in the plenum chamber (station 0) were determined by four stagnation-pressure probes and four stagnation thermocouples. The inlet static pressure was measured by averaging the readings from 12 taps, six on the inner and six on the outer wall of the annulus about 1 inch upstream of the stator blade leading edges (station 1). The outlet static pressure was measured in a similar manner using 12 taps at station 5, about 1.9 inches downstream of the rotor blade trailing edges. At stations 1 and 5 the static taps were equally spaced around the annulus in planes perpendicular to the turbine axis. The exit stagnation temperature was obtained by averaging the readings from four stagnation thermocouples located in the 18-inch-diameter exhaust duct (station 6), where only small gradients in temperature exist. Heat-transfer calculations show a negligible change in temperature between stations 5 and 6.

Torque was measured with a commercial springless dynamometer scale. Air flow was measured with a submerged flat-plate orifice installed in the 24-inch inlet duct to conform with the specifications in reference 11. An electronic events-per-unit-time meter was used to measure the turbine rotative speed. Absolute rotor-exit flow angles were measured with a total-pressure claw probe mounted in a self-aligning actuator about 1.9 inches downstream of the rotor. Measurements of the flow angle were transmitted to an X-Y recorder and plotted against the radial distance traversed by the probe.

Experimental Procedure and Calculations

Over-all performance data were taken at nominal values of total-pressure ratio p_1^t/p_5^t from 1.3 to the maximum obtainable, while the wheel speed was varied from 60 to 110 percent of equivalent design speed in 5-percent intervals (approx. 7,200 to 13,250 rpm). The absolute inlet pressure was set at 50 inches of mercury (24.6 lb/sq in. abs), and the temperature was about 80° F.

The turbine is rated on the basis of two different calculated over-all total-pressure ratios. The axial total-pressure ratio is based on the rotor-exit total pressure $p_{x,5}^t$, which is the sum of the static pressure plus the dynamic pressure corresponding to the axial component of the exit velocity $V_{x,5}$. The actual total-pressure ratio is based on the rotor-exit total pressure p_5^t , which is the sum of the static pressure plus the dynamic pressure corresponding to the absolute velocity at station 5, V_5 .

At the inlet and outlet of the turbine the total pressure is calculated from continuity considerations. Using measured values of weight flow, inlet static pressure and total temperature, and annulus area, the inlet total pressure may be obtained from the following equation, which is a rearranged form of equation (2) of reference 12:

$$\frac{w\sqrt{T_1^t}}{p_1 A_{an,1}} = \sqrt{\frac{2\gamma g}{(\gamma - 1)R}} \left\{ \left[\left(\frac{p_1^t}{p_1} \right)^{\frac{\gamma-1}{\gamma}} - 1 \right] + \left[\left(\frac{p_1^t}{p_1} \right)^{\frac{\gamma-1}{\gamma}} - 1 \right]^2 \right\}^{1/2} \quad (4)$$

The outlet rating total pressure is calculated from the following equation, which is a rearranged form of equation (3) of reference 12:

$$\frac{w\sqrt{T_6^t}}{p_5 A_{an,5}} = \sqrt{\frac{2\gamma g}{(\gamma - 1)R}} \left\{ \left[\left(\frac{p_{5,x}^t}{p_5} \right)^{\frac{\gamma-1}{\gamma}} - 1 \right] + \left[\frac{\left(\frac{p_{5,x}^t}{p_5} \right)^{\frac{\gamma-1}{\gamma}} - 1}{\cos \alpha_5} \right]^2 \right\}^{1/2} \quad (5)$$

The outlet absolute total pressure is calculated from

$$\frac{w\sqrt{T_6}}{p_5 A_{an,5} \cos \alpha_5} = \sqrt{\frac{2\gamma g}{(\gamma - 1)R}} \left\{ \left[\left(\frac{p'_5}{p_5} \right)^{\frac{\gamma-1}{\gamma}} - 1 \right] + \left[\left(\frac{p'_5}{p_5} \right)^{\frac{\gamma-1}{\gamma}} - 1 \right]^2 \right\}^{1/2} \quad (6)$$

The turbine efficiency was calculated by taking the ratio of the actual work output obtained from measurements of weight flow, torque, and turbine rotative speed to the ideal enthalpy drop calculated from the measured inlet temperature and the ratio of inlet to outlet total pressure as obtained from the total pressures calculated in equations (4) to (6).

RESULTS AND DISCUSSION

The over-all performance map for the subject turbine based on the actual total-pressure ratio is presented in figure 8(a). The equivalent specific work $\Delta h' / \omega_{cr}$ is plotted against the weight-flow - mean-blade-speed parameter swU_m / δ with the actual total-pressure ratio p'_1 / p'_5 , percent equivalent design blade speed, and the brake internal rating efficiency as parameters. At equivalent design specific work output and equivalent design blade speed, the brake internal efficiency is 0.875, and the weight flow is about 0.9 percent less than the design value. The work output at the point of limiting blade loading and design blade speed is 21.4 Btu per pound which is 4 percent greater than the design value. A maximum efficiency of 0.883 occurs at equivalent design blade speed and at a value of specific work output about 4 percent less than design. The efficiency is greater than 0.87 over a large portion of the performance map.

The turbine over-all performance map based on the axial total-pressure ratio is presented in figure 8(b). The brake internal rating efficiency at equivalent design blade speed and work output is 0.870, indicating that about 1/2 point in turbine efficiency was lost in the whirl velocity component energy downstream of the rotor. This loss in available work is comparable to the predicted energy loss of 0.8 percent.

The variation of the static pressure on the annulus walls downstream of the stator and rotor blades (stations 3 and 5) with the actual over-all total-pressure ratio at equivalent design blade speed is presented in figure 9(a). An average of hub and tip values of static pressure downstream of the rotor is used because the two values are very nearly equal. The variation in weight flow is shown in figure 9(b). This

figure indicates that the rotor blades become choked at a pressure ratio of about 2.1. At total-pressure ratios greater than this, the static pressures at station 3 remain constant. A comparison of the static pressures at the exit of the stator hub with those at the rotor exit indicates a slight static-pressure rise across the rotor blades at the hub even at the point of design work output, although the design velocity diagrams require a static-pressure drop across the rotor hub. This difference between the measured and the design condition may be partly due to inaccurate measurements of the static pressure at the hub exit of the stator blades. The supersonic velocities in this region may exist in a pattern such that the measured pressures are not typical of the average flow conditions.

The rapid decrease in the pressure downstream of the rotor at total-pressure ratios greater than 2.2 indicates the supersonic expansion that precedes limiting blade loading.

The performance map based on the axial total-pressure ratio (fig. 8(b)) indicates that the efficiency drops off rapidly as limiting blade loading is approached in the rotor at design blade speed. The supersonic velocities and the attendant shock losses on the downstream portion of the rotor blade suction surface apparently cause high losses. The rating efficiency drops 5 points from 0.87 to 0.82 as the pressure ratio is increased from the condition of design work output to the point of maximum blade loading.

The effective rotor blade momentum thickness was calculated with the method presented in reference 13. In order to compare the value of the ratio of effective rotor blade momentum thickness to mean camber length $\bar{\theta}_{tot}/l$ for the subject turbine with the values for the six transonic turbines presented in reference 13, a slight correction for Reynolds number was made using equation (5) of reference 6. The Reynolds number for the six transonic turbines was used as the reference value. The resulting value of $\bar{\theta}_{tot}/l$ of 0.0104, when plotted with the average design total diffusion parameter of 0.21 as shown in figure 10, agrees reasonably well with the data for the six transonic turbines.

SUMMARY OF RESULTS

The design and performance of a turbine having high weight flow per unit frontal area and high specific work output are presented. The subject turbine had a high relative inlet blade Mach number at the rotor hub and was designed for low diffusion on both the suction and pressure surfaces of the rotor blades. The following results were obtained over a range of operating conditions:

1. The brake internal efficiency based on the actual total-pressure ratio at the equivalent design blade speed and specific work output was

0.875, which is almost as high as that obtained for conservatively designed turbines. The efficiency based on the axial total-pressure ratio at this point was 0.870.

2. By running the turbine at the point of limiting rotor blade loading and equivalent design blade speed, a work output 4 percent greater than the design value was obtained, but the over-all efficiency was 0.05 lower than at the design point. This increase in loss was apparently caused by the shock waves and attendant boundary-layer losses on the portion of the rotor blade suction surface downstream of the channel exit.

3. The calculated value of the ratio of effective rotor blade momentum thickness to mean camber length of 0.0104 agrees reasonably well with the values previously obtained for transonic turbines.

Lewis Flight Propulsion Laboratory
National Advisory Committee for Aeronautics
Cleveland, Ohio, July 27, 1956

APPENDIX A

SYMBOLS

| | |
|-------------|---|
| A_{an} | annular area, sq ft |
| a_{cr} | critical velocity of sound, ft/sec |
| c | chord length, ft |
| c_p | specific heat at constant pressure, Btu/lb-°R |
| D_p | pressure-surface diffusion parameter, $\frac{\text{blade inlet relative velocity} - \text{minimum blade surface relative velocity}}{\text{blade inlet relative velocity}}$ |
| D_s | suction-surface diffusion parameter, $\frac{\text{maximum blade surface relative velocity} - \text{blade outlet relative velocity}}{\text{maximum blade surface relative velocity}}$ |
| D_{tot} | sum of suction- and pressure-surface diffusion parameters, $D_p + D_s$ |
| $f(w)$ | weight-flow parameter, $\frac{w}{\rho'' \sqrt{2gJc_p T''}}$, ft ² |
| g | acceleration due to gravity, 32.17 ft/sec ² |
| $\Delta h'$ | specific work output, Btu/lb |
| J | mechanical equivalent of heat, 778.2 ft-lb/Btu |
| K | proportionality factor in eq. (B1) |
| l | length of mean camber line, ft |
| l_o | distance from suction to pressure surface along a line in a tangential direction, ft |
| n_R | number of rotor blades |
| n_S | number of stator blades |
| p | absolute pressure, lb/sq ft |

- R gas constant, 53.35 ft-lb/(lb)(°R)
- r radius, ft
- s blade spacing, ft
- T absolute temperature, °R
- t trailing-edge thickness, ft
- U blade velocity, ft/sec
- V absolute gas velocity, ft/sec
- W relative gas velocity, ft/sec
- w weight flow, lb/sec
- α absolute gas-flow angle measured from axial direction
- β relative gas-flow angle measured from axial direction
- Γ circulation, sq ft/sec
- γ ratio of specific heats
- γ° blade-chord angle, angle between blade chord and axial direction, deg
- δ ratio of inlet-air total pressure to NACA standard sea-level pressure of 2116 lb/sq ft, p_1/p^*

ϵ function of $\gamma, \frac{\gamma^*}{\gamma} \left[\frac{\left(\frac{\gamma+1}{2}\right)^{\frac{\gamma}{\gamma-1}}}{\frac{\gamma^*}{\left(\frac{\gamma^*+1}{2}\right)^{\gamma^*-1}}} \right]$

- η brake internal efficiency defined as ratio of turbine work (based on torque, weight flow, and speed measurements) to ideal work (based on inlet total temperature, and inlet and outlet total pressure, both defined as sum of static pressure and pressure corresponding to gas velocity)

- η_x brake internal rating efficiency defined as ratio of turbine work (based on torque, weight flow, and speed measurements) to ideal work (based on inlet total temperature, and inlet and outlet total pressure, both defined as sum of static pressure and pressure corresponding to axial component of velocity)
- θ_{cr}^2 squared ratio of critical velocity at turbine inlet to critical velocity at NACA standard sea-level temperature $(a'_{cr,l}/a^*_{cr})^2$
- $\bar{\theta}_{tot}$ effective rotor blade momentum thickness based on turbine over-all performance, ft
- ρ gas density, lb/cu ft

Subscripts:

- h hub
- m mean
- r any radius
- t tip
- tot total
- u tangential
- x axial
- 0 station in plenum chamber (see fig. 7)
- 1 station upstream of stator
- 2 station at trailing edge of stator
- 3 station at free-stream condition between stator and rotor
- 4 station at trailing edge of rotor
- 5 station downstream of rotor
- 6 station in 18-inch-diameter exhaust duct (see fig. 7)

Superscripts:

- * NACA standard conditions
- ' stagnation state
- " relative stagnation state

APPENDIX B

CALCULATION OF STATOR AXIAL CHORD TO APPROXIMATE CONSTANT

BLADE LOADING OVER BLADE HEIGHT

In order to reduce the blade surface boundary-layer losses by reducing the blade surface area and still control the diffusion on the blade surfaces, an attempt was made to design the stator with constant blade loading over the blade height. In order to approximate the relative values of axial chord length at hub, mean, and tip sections, a blade-loading criterion similar to that developed in reference 8 was used. It was desired to hold constant the ratio of the design blade loading to that obtained when the exit static pressure p_2 is effective over the entire blade suction surface while the inlet total pressure is effective over the pressure surface. Thus, in the momentum equation for the stator

$$\left(\frac{\rho V_x}{\rho' a_{cr}'} \right)_{2,r} s_r \left(\frac{V_u}{a_{cr}'} \right)_{2,r} = Kg \left(\frac{c_{x,r}}{\rho_2' a_{cr,2}'} \right) p_1^i - p_{2,r} \quad (B1)$$

the proportionality factor K is held constant over the blade height. The ratio of the axial chord at any radius can then be related to that at the mean section by the equation

$$\frac{c_{x,r}}{c_{x,m}} = \frac{\frac{s_r \left(\frac{\rho V_x}{\rho' a_{cr}'} \right)_{2,r} \left(\frac{V_u}{a_{cr}'} \right)_{2,r}}{1 - \frac{p_{2,r}}{p_1^i}}}{\frac{s_m \left(\frac{\rho V_x}{\rho' a_{cr}'} \right)_{2,m} \left(\frac{V_u}{a_{cr}'} \right)_{2,m}}{1 - \frac{p_{2,m}}{p_1^i}}} \quad (B2)$$

For free-vortex-velocity conditions,

$$r \left(\frac{V_u}{a_{cr}'} \right)_r = \text{constant}$$

$$\left(\frac{V_x}{a_{cr}'} \right)_r = \text{constant}$$

Substituting these relations into equation (B2) gives

$$\frac{c_{x,r}}{c_{x,m}} = \frac{\left(\frac{\rho}{\rho'}\right)_{2,r} \left(1 - \frac{p_{2,m}}{p_1'}\right)}{\left(\frac{\rho}{\rho'}\right)_{2,m} \left(1 - \frac{p_{2,r}}{p_1'}\right)} \quad (B3)$$

Having set the chord at the mean blade section, the chord lengths at the hub and tip sections are calculated from equation (B3).

APPENDIX C

CALCULATION OF STATOR-EXIT ANGLE α_2

The angle α_2 at the stator trailing edge was calculated using the following assumptions:

- (1) No change in the tangential component of velocity occurs between stations 2 and 3.
- (2) The trailing edge lies in a radial plane.
- (3) Axisymmetric flow exists.
- (4) The conditions of simplified radial equilibrium are satisfied at stations 2 and 3.
- (5) Free-vortex flow exits from hub to tip at station 3.
- (6) A total-pressure ratio p_3/p_2 of 0.99 is assumed.

From assumptions (1) and (5), the tangential critical velocity ratio $(V_u/a'_{cr})_2$ at station 2 was determined at each radius from the design velocity diagrams. However, in order to satisfy the requirements of both simplified radial equilibrium and continuity, an iterative procedure had to be used to find the absolute velocity V_2 and the angle α_2 . With an assumed value of α_2 at the hub section, values of α_2 were found at eight other equally spaced radial stations by numerical integration of the following equation, which expresses the condition of simplified radial equilibrium (eq. (B3), ref. 7):

$$\frac{V_{u,h}}{\sin \alpha_{2,h}} \frac{\sin \alpha_{2,r}}{V_{u,r}} = e^{\int_{r_h}^r \frac{\sin^2 \alpha_{2,r}}{r} dr} \quad (C1)$$

For these calculated values of angle and velocity, the weight flow w was calculated from the equation

$$w = n_g \int_{r_h}^{r_t} (\rho V_x)_2 \left(s - \frac{t}{\cos \alpha_2} \right) dr \quad (C2)$$

The final distribution of α_2 was obtained through an iterative process such that the weight flow calculated in equation (C2) agreed with the design value within one-tenth of 1 percent.

APPENDIX D

CALCULATION OF MEAN STREAMLINES IN ROTOR BLADE PASSAGE

SATISFYING FREE-VORTEX CONDITIONS

With a given blade profile at the hub radial station and an assumed velocity distribution on the mean streamline at that station, the mean streamlines and corresponding velocity distributions were calculated at the mean and tip stations in a manner such that free-vortex conditions were satisfied along radial elements.

Using values of the blade speed $(U/a_{cr}^i)_{3,r}$ and the tangential critical velocity ratio $(V_u/a_{cr}^i)_{3,r}$ from the velocity diagrams, the ratio of relative critical velocity to absolute critical velocity was calculated at each radial station from the relation

$$\left(\frac{a_{cr}''}{a_{cr}^i}\right)_{3,r} = \sqrt{1 - \frac{\gamma - 1}{\gamma + 1} \left(\frac{U}{a_{cr}^i}\right)_{3,r} \left[2 \left(\frac{V_u}{a_{cr}^i}\right)_{3,r} - \left(\frac{U}{a_{cr}^i}\right)_{3,r} \right]} \quad (D1)$$

With the assumed values of critical velocity ratio $(W/a_{cr}'')_h$ and flow angle β_h at each of 11 axial stations at the hub, the following procedure was used:

(1) The axial and tangential components of critical velocity ratio at each axial station on the hub mean streamline were calculated with the following relations:

$$\left(\frac{W}{a_{cr}^i}\right)_h = \left(\frac{W}{a_{cr}''}\right)_h \left(\frac{a_{cr}''}{a_{cr}^i}\right)_{3,h} \quad (D2)$$

$$\left(\frac{W_u}{a_{cr}^i}\right)_h = \left(\frac{W}{a_{cr}^i}\right)_h \sin \beta_h \quad (D3)$$

$$\left(\frac{W_x}{a_{cr}^i}\right)_h = \left(\frac{W}{a_{cr}^i}\right)_h \cos \beta_h \quad (D4)$$

$$\left(\frac{V_u}{a_{cr}^i}\right)_h = \left(\frac{W_u}{a_{cr}^i}\right)_h + \left(\frac{U}{a_{cr}^i}\right)_{3,h} \quad (D5)$$

(2) Then, at the mean and tip stations along radial lines at each of the axial stations through the rotor, the tangential and axial components of the critical velocity ratio along the mean streamlines were calculated from the free-vortex relations

$$\left(\frac{V_u}{a_{cr}^i}\right)_r = \frac{r_h}{r} \left(\frac{V_u}{a_{cr}^i}\right)_h \quad (D6)$$

$$\left(\frac{W_u}{a_{cr}^i}\right)_r = \left(\frac{V_u}{a_{cr}^i}\right)_r - \left(\frac{U}{a_{cr}^i}\right)_{3,r} \quad (D7)$$

$$\left(\frac{W_x}{a_{cr}^i}\right)_r = \left(\frac{W_x}{a_{cr}^i}\right)_h \quad (D8)$$

(3) The critical velocity ratios and flow angles on the mean streamlines relative to the rotor were determined at the mean and tip radial stations at each of the 11 axial stations from the following relations:

$$\left(\frac{W_u}{a_{cr}^n}\right)_r = \left(\frac{W_u}{a_{cr}^i}\right)_r \left(\frac{a_{cr}^i}{a_{cr}^n}\right)_{3,r} \quad (D9)$$

$$\left(\frac{W_x}{a_{cr}^n}\right)_r = \left(\frac{W_x}{a_{cr}^i}\right)_r \left(\frac{a_{cr}^i}{a_{cr}^n}\right)_{3,r} \quad (D10)$$

$$\beta_r = \tan^{-1} \frac{\left(\frac{W_u}{a_{cr}^n}\right)_r}{\left(\frac{W_x}{a_{cr}^n}\right)_r} \quad (D11)$$

REFERENCES

1. Heller, Jack A., Whitney, Rose L., and Cavicchi, Richard H.: Experimental Investigation of a Conservatively Designed Turbine at Four Rotor-Blade Solidities. NACA RM E52C17, 1952.
2. Stewart, Warner L., Wong, Robert Y., and Evans, David G.: Design and Experimental Investigation of Transonic Turbine with Slight Negative Reaction Across Rotor Hub. NACA RM E53L29a, 1954.

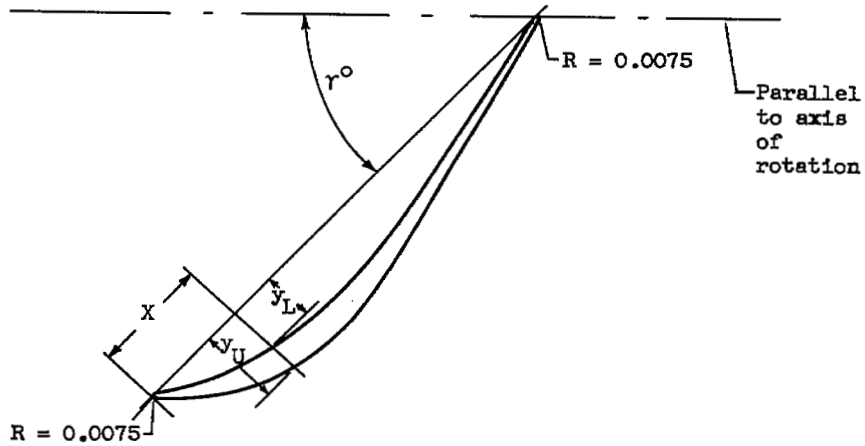
3. Whitney, Warren J., Monroe, Daniel E., and Wong, Robert Y.: Investigation of Transonic Turbine Designed for Zero Diffusion of Suction-Surface Velocity. NACA RM E54F23, 1954.
4. Miser, James W., Stewart, Warner L., and Monroe, Daniel E.: Effect of High Rotor Pressure-Surface Diffusion on Performance of a Transonic Turbine. NACA RM E55H29a, 1955.
5. Hauser, Cavour H., and Plohr, Henry W.: Two-Dimensional Cascade Investigation of the Maximum Exit Tangential Velocity Component and Other Flow Conditions at the Exit of Several Turbine-Blade Designs at Supercritical Pressure Ratios. NACA RM E51F12, 1951.
6. Miser, James W., Stewart, Warner L., and Whitney, Warren J.: Analysis of Turbomachine Viscous Losses Affected by Changes in Blade Geometry. NACA RM E56F21, 1956.
7. Miser, James W., Stewart, Warner L., and Wong, Robert Y.: Effect of a Reduction in Stator Solidity on Performance of a Transonic Turbine. NACA RM E55L09a, 1956.
8. Zweifel, O.: Optimum Blade Pitch for Turbo-Machines with Special Reference to Blades of Great Curvature. The Eng. Digest, vol. 7, no. 11, Nov. 1946, pp. 358-360; cont., vol. 7, no. 12, Dec. 1946, pp. 381-383.
9. Huppert, M. C., and MacGregor, Charles: Comparison Between Predicted and Observed Performance of Gas-Turbine Stator Blade Designed for Free-Vortex Flow. NACA TN 1810, 1949.
10. Alpert, Sumner: Design Method for Two-Dimensional Channels for Compressible Flow with Application to High-Solidity Cascades. NACA TN 1931, 1949.
11. Anon.: Fluid Meters, Their Theory and Application. A.S.M.E. Res. Pub., Fourth ed., pub. by A.S.M.E. (New York), 1937.
12. Stewart, Warner L., Schum, Harold J., and Whitney, Warren J.: Investigation of Turbines for Driving Supersonic Compressors. I - Design and Performance of First Configuration. NACA RM E52C25, 1952.
13. Stewart, Warner L., Whitney, Warren J., and Miser, James W.: Use of Effective Momentum Thickness in Describing Turbine Rotor-Blade Losses. NACA RM E56B29, 1956.

5008

CW-4

TABLE I. - BLADE-SECTION COORDINATES

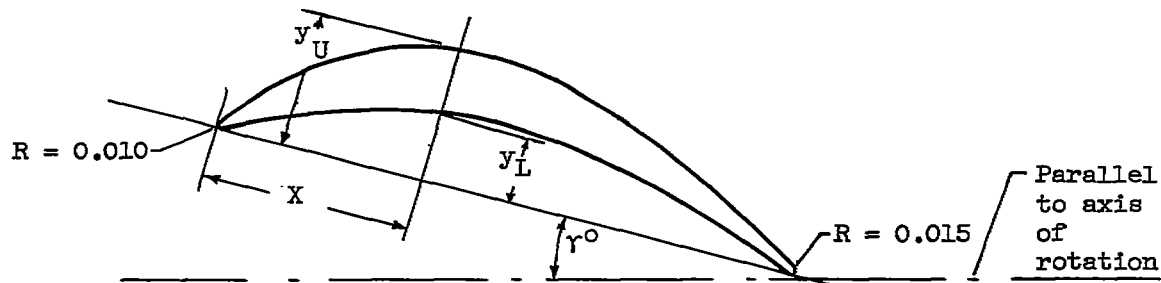
(a) Stator



| | Hub | | Mean | | Tip | |
|--------|---------------------|-------------|---------------------|-------------|---------------------|-------------|
| | $\gamma^o = 54.7^o$ | | $\gamma^o = 46.4^o$ | | $\gamma^o = 40.0^o$ | |
| | $r/r_t = 0.60$ | | $r/r_t = 0.80$ | | $r/r_t = 1.00$ | |
| X, in. | y_U , in. | y_L , in. | y_U , in. | y_L , in. | y_U , in. | y_L , in. |
| 0 | 0.0075 | 0.0075 | 0.0075 | 0.0075 | 0.0075 | 0.0075 |
| .10 | .114 | .045 | .100 | .051 | .094 | .053 |
| .20 | .168 | .080 | .174 | .103 | .163 | .107 |
| .30 | .185 | .102 | .226 | .143 | .223 | .154 |
| .40 | .172 | .113 | .261 | .170 | .270 | .191 |
| .50 | .152 | .112 | .280 | .187 | .307 | .221 |
| .60 | .131 | .100 | .283 | .198 | .335 | .241 |
| .70 | .112 | .084 | .273 | .200 | .352 | .254 |
| .80 | .091 | .066 | .255 | .196 | .361 | .260 |
| .90 | .071 | .049 | .232 | .183 | .360 | .261 |
| 1.00 | .051 | .029 | .208 | .165 | .349 | .255 |
| 1.10 | .030 | .011 | .184 | .146 | .333 | .246 |
| 1.179 | .0075 | .0075 | ---- | ---- | ---- | ---- |
| 1.20 | ---- | ---- | .160 | .125 | .310 | .233 |
| 1.30 | ---- | ---- | .136 | .103 | .283 | .217 |
| 1.40 | ---- | ---- | .111 | .081 | .257 | .198 |
| 1.490 | ---- | ---- | ---- | ---- | ---- | ---- |
| 1.50 | ---- | ---- | .086 | .060 | .231 | .177 |
| 1.60 | ---- | ---- | .062 | .038 | .206 | .155 |
| 1.70 | ---- | ---- | .037 | .017 | .179 | .133 |
| 1.789 | ---- | ---- | .0075 | .0075 | ---- | ---- |
| 1.80 | ---- | ---- | ---- | ---- | .152 | .112 |
| 1.90 | ---- | ---- | ---- | ---- | .126 | .091 |
| 2.00 | ---- | ---- | ---- | ---- | .100 | .068 |
| 2.069 | ---- | ---- | ---- | ---- | ---- | ---- |
| 2.10 | ---- | ---- | ---- | ---- | .074 | .046 |
| 2.20 | ---- | ---- | ---- | ---- | .048 | .025 |
| 2.30 | ---- | ---- | ---- | ---- | .022 | .006 |
| 2.335 | ---- | ---- | ---- | ---- | .0075 | .0075 |

TABLE I. - Concluded. BLADE-SECTION COORDINATES

(b) Rotor



| X, in. | Hub | | Mean | | Tip | |
|--------|-------------------------|----------------------|-------------------------|----------------------|-------------------------|----------------------|
| | γ ⁰ = -8.6° | | γ ⁰ = 15.4° | | γ ⁰ = 32.1° | |
| | r/r _t = 0.60 | | r/r _t = 0.80 | | r/r _t = 1.00 | |
| | y _L , in. | y _U , in. | y _L , in. | y _U , in. | y _L , in. | y _U , in. |
| 0 | 0.010 | 0.010 | 0.010 | 0.010 | 0.010 | 0.010 |
| .025 | .010 | .038 | .007 | .043 | .002 | .039 |
| .100 | .073 | .108 | .046 | .123 | .012 | .101 |
| .200 | .142 | .198 | .090 | .209 | .025 | .159 |
| .300 | .195 | .277 | .125 | .269 | .037 | .194 |
| .400 | .236 | .340 | .150 | .304 | .048 | .213 |
| .500 | .263 | .384 | .167 | .317 | .059 | .221 |
| .600 | .277 | .406 | .174 | .311 | .070 | .219 |
| .700 | .276 | .408 | .170 | .293 | .076 | .211 |
| .800 | .263 | .389 | .157 | .263 | .080 | .198 |
| .900 | .235 | .349 | .138 | .227 | .079 | .182 |
| 1.000 | .190 | .289 | .112 | .185 | .073 | .163 |
| 1.100 | .130 | .209 | .079 | .139 | .063 | .141 |
| 1.200 | .057 | .117 | .042 | .089 | .049 | .115 |
| 1.270 | .001 | .044 | ---- | ---- | ---- | ---- |
| 1.285 | ---- | ---- | .007 | .044 | ---- | ---- |
| 1.291 | .015 | .015 | ---- | ---- | ---- | ---- |
| 1.300 | ---- | ---- | ---- | ---- | .033 | .086 |
| 1.320 | ---- | ---- | .015 | .015 | ---- | ---- |
| 1.400 | ---- | ---- | ---- | ---- | .016 | .056 |
| 1.475 | ---- | ---- | ---- | ---- | .001 | .033 |
| 1.498 | ---- | ---- | ---- | ---- | .015 | .015 |

5008

CN-4 back

TABLE II. - SURFACE DIFFUSION PARAMETERS FOR
STATOR AND ROTOR BLADES

| Blade | Section | Blade surface diffusion parameters | | |
|--------|---------|------------------------------------|-------------------------|------------------|
| | | Suction surface, D_s | Pressure surface, D_p | Total, D_{tot} |
| Stator | Hub | 0.26 | 0 | 0.26 |
| | Mean | .18 | .07 | .25 |
| | Tip | .10 | .29 | .39 |
| Rotor | Hub | 0 | 0.27 | 0.27 |
| | Mean | .06 | .12 | .18 |
| | Tip | .12 | .06 | .18 |

5008

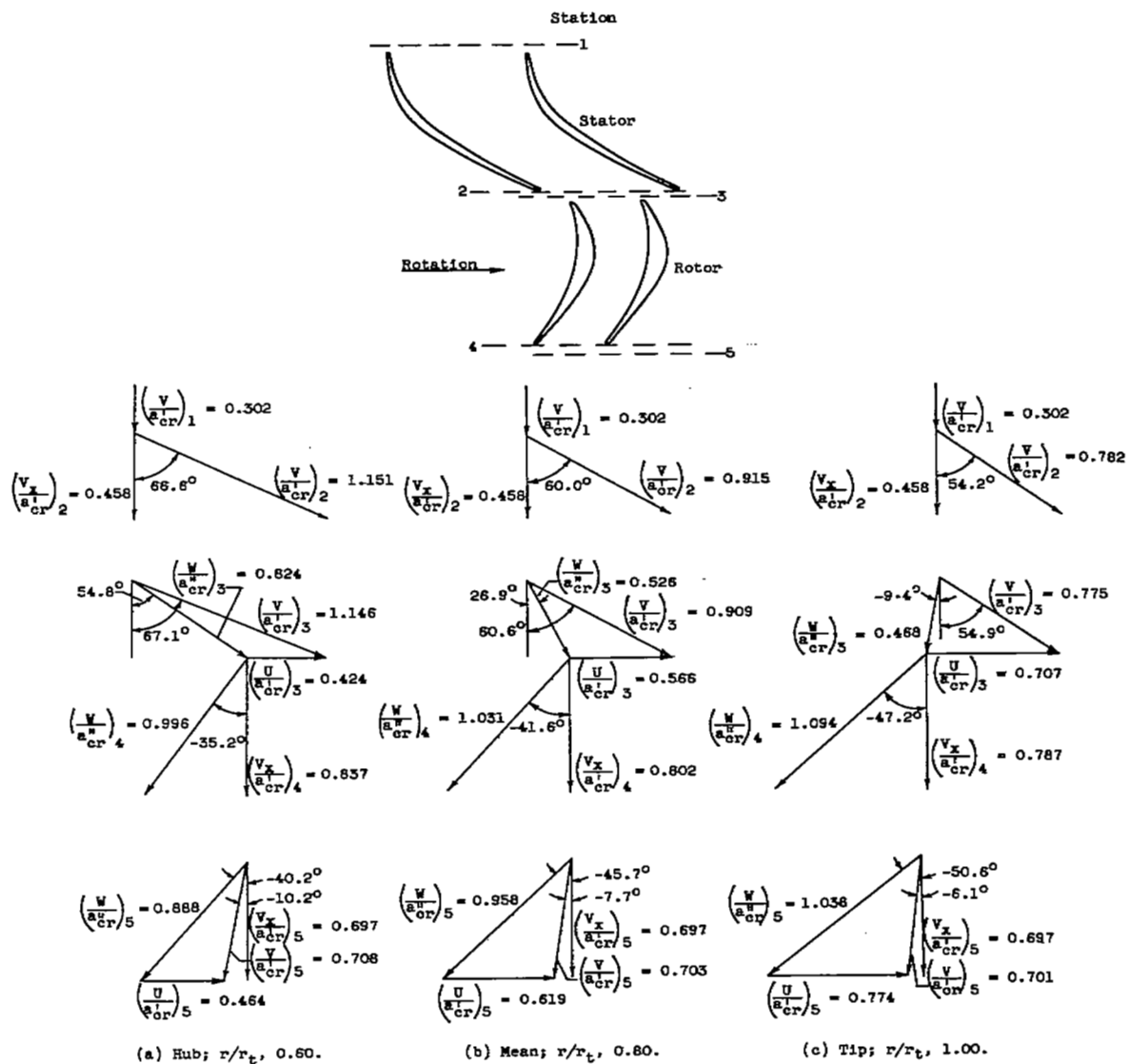


Figure 1. - Turbine velocity diagrams.

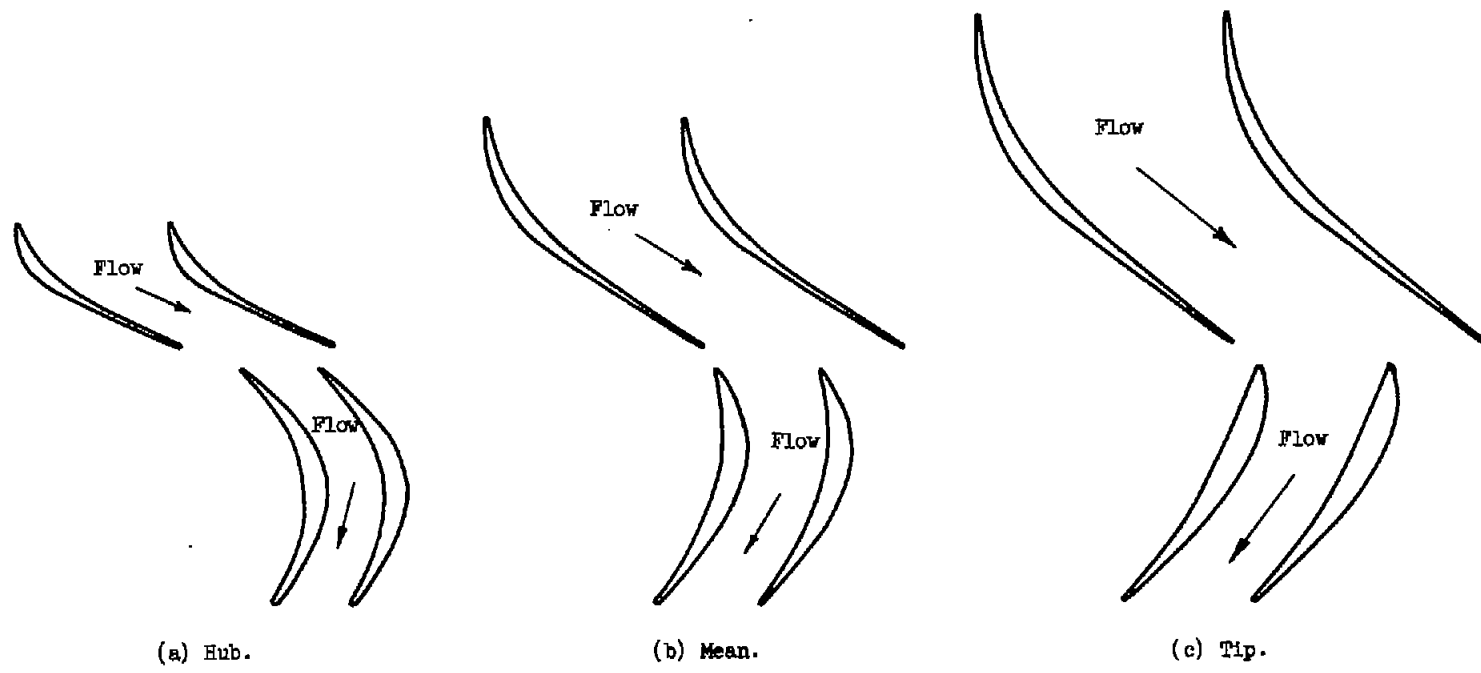
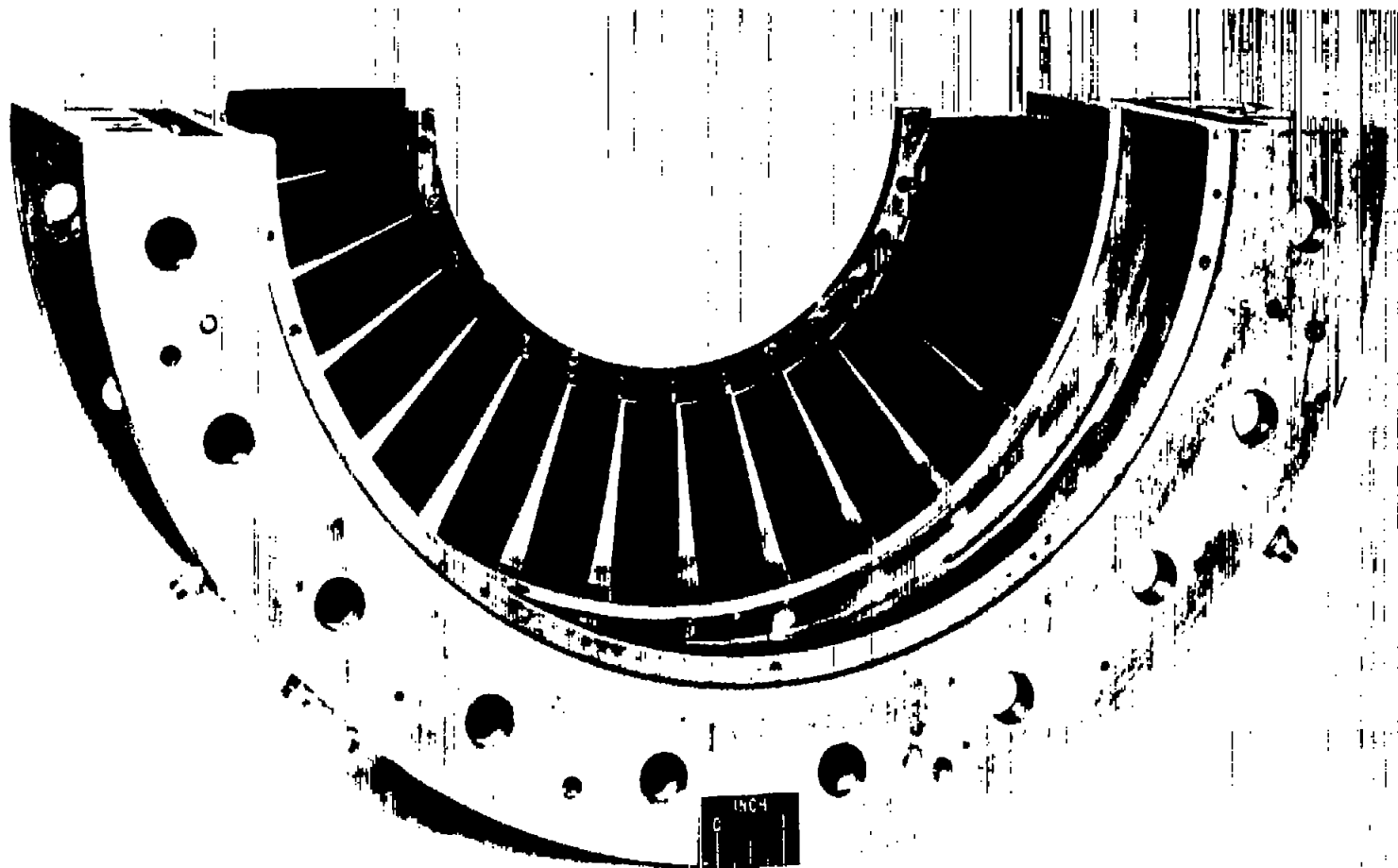


Figure 2.- Stator and rotor blade passages and profiles.



C-41121

Figure 3. - Photograph of half of stator casing viewed from downstream.

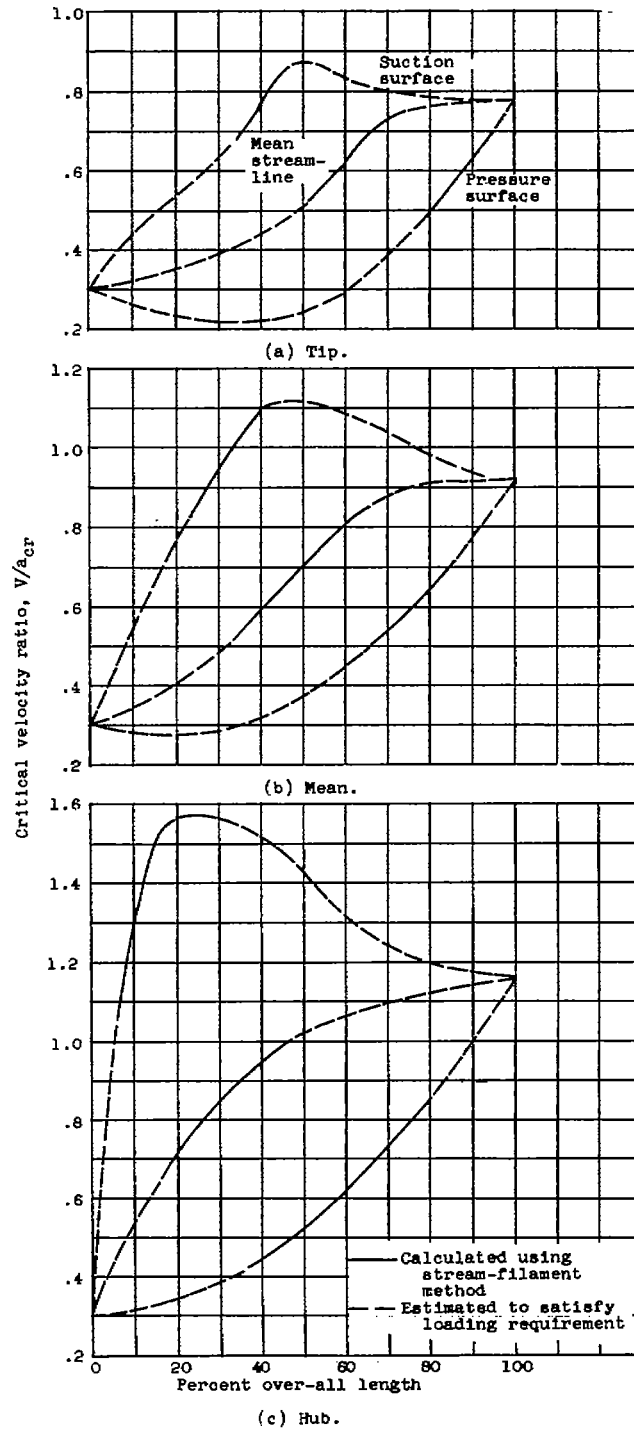
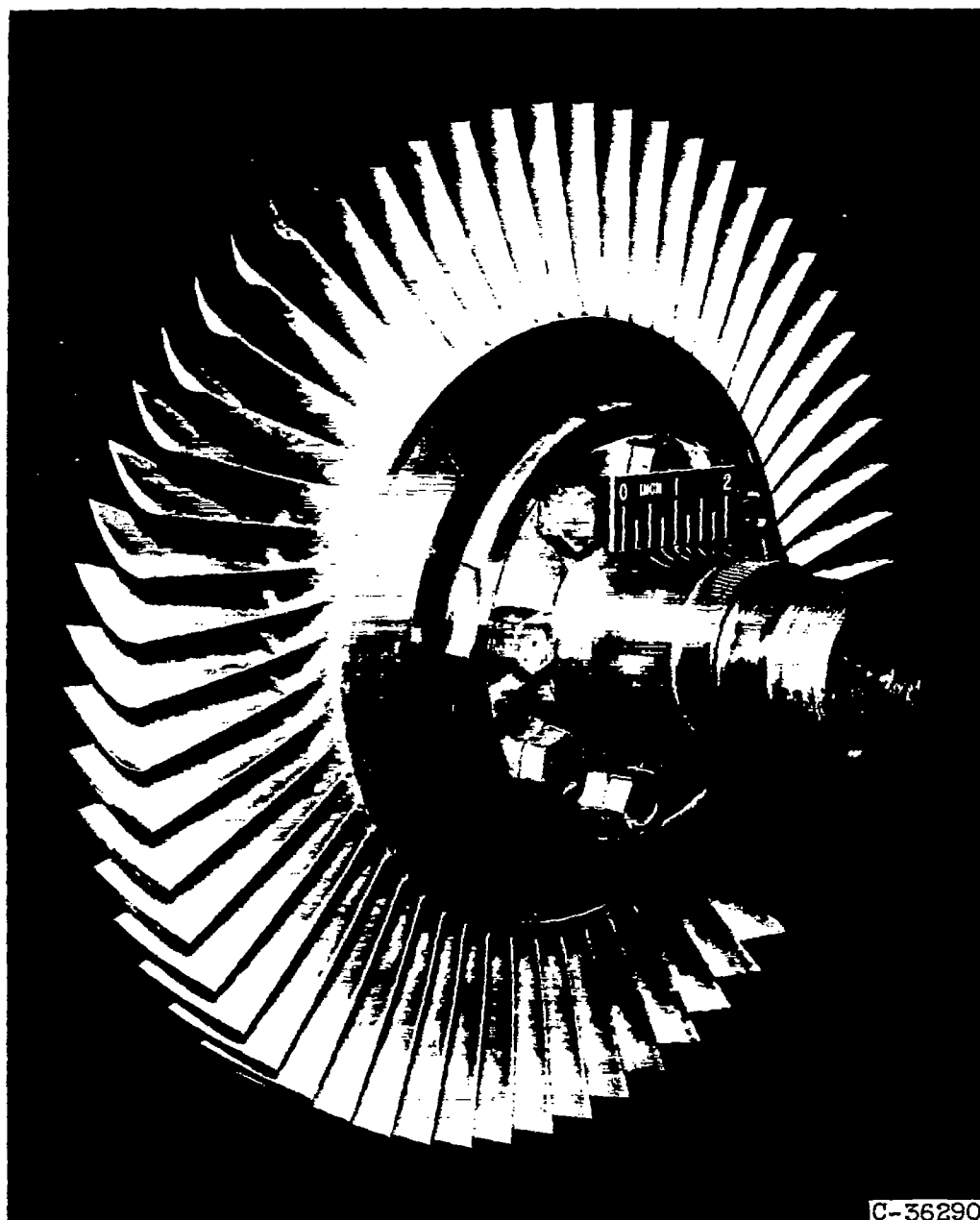


Figure 4. - Design stator mean streamline and surface velocity distributions at hub, mean, and tip sections as function of percent over-all length.

5008

CW-5



C-36290

Figure 5. - Turbine rotor.

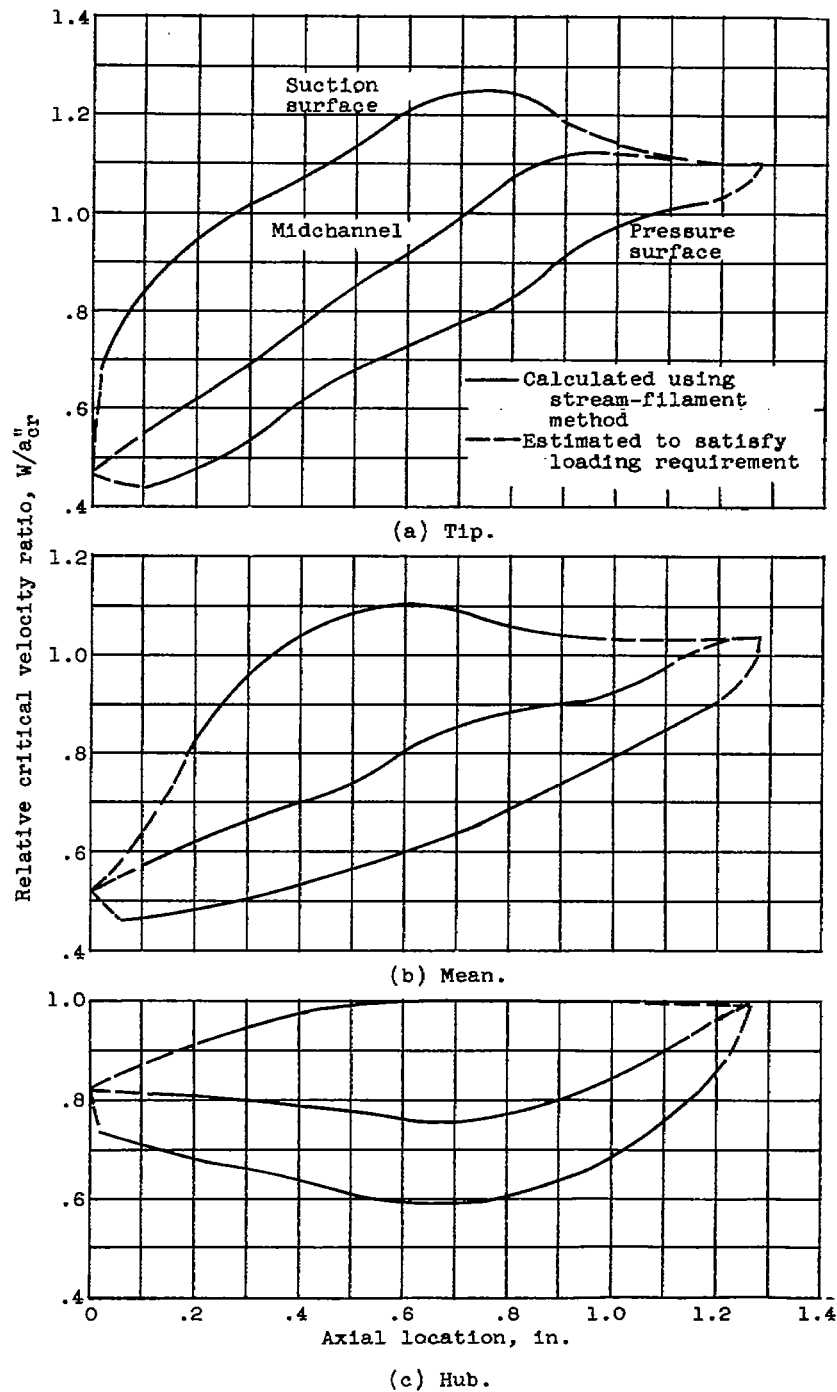


Figure 6. - Design rotor midchannel and surface velocity distributions at hub, mean, and tip sections as function of axial location.

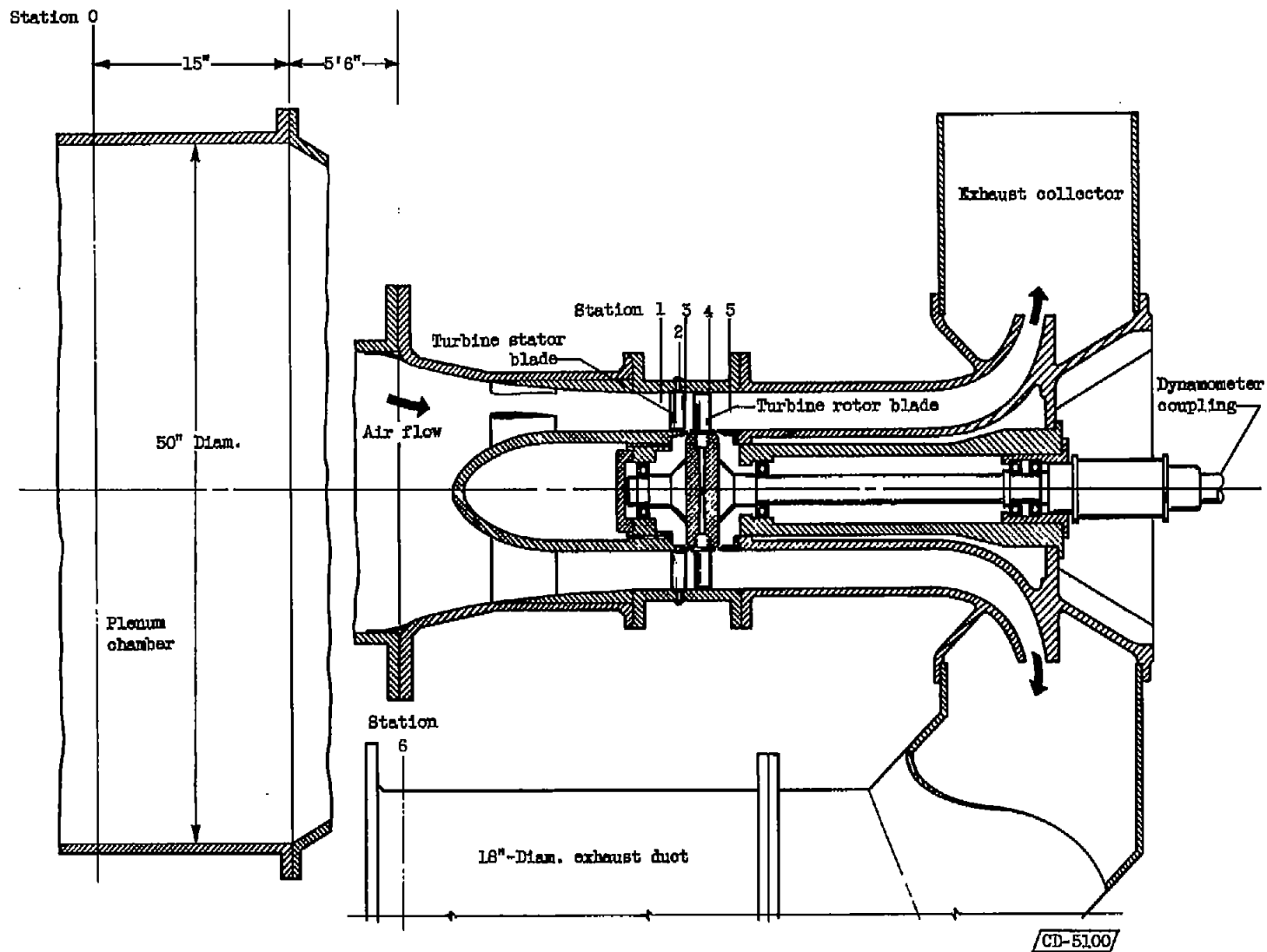
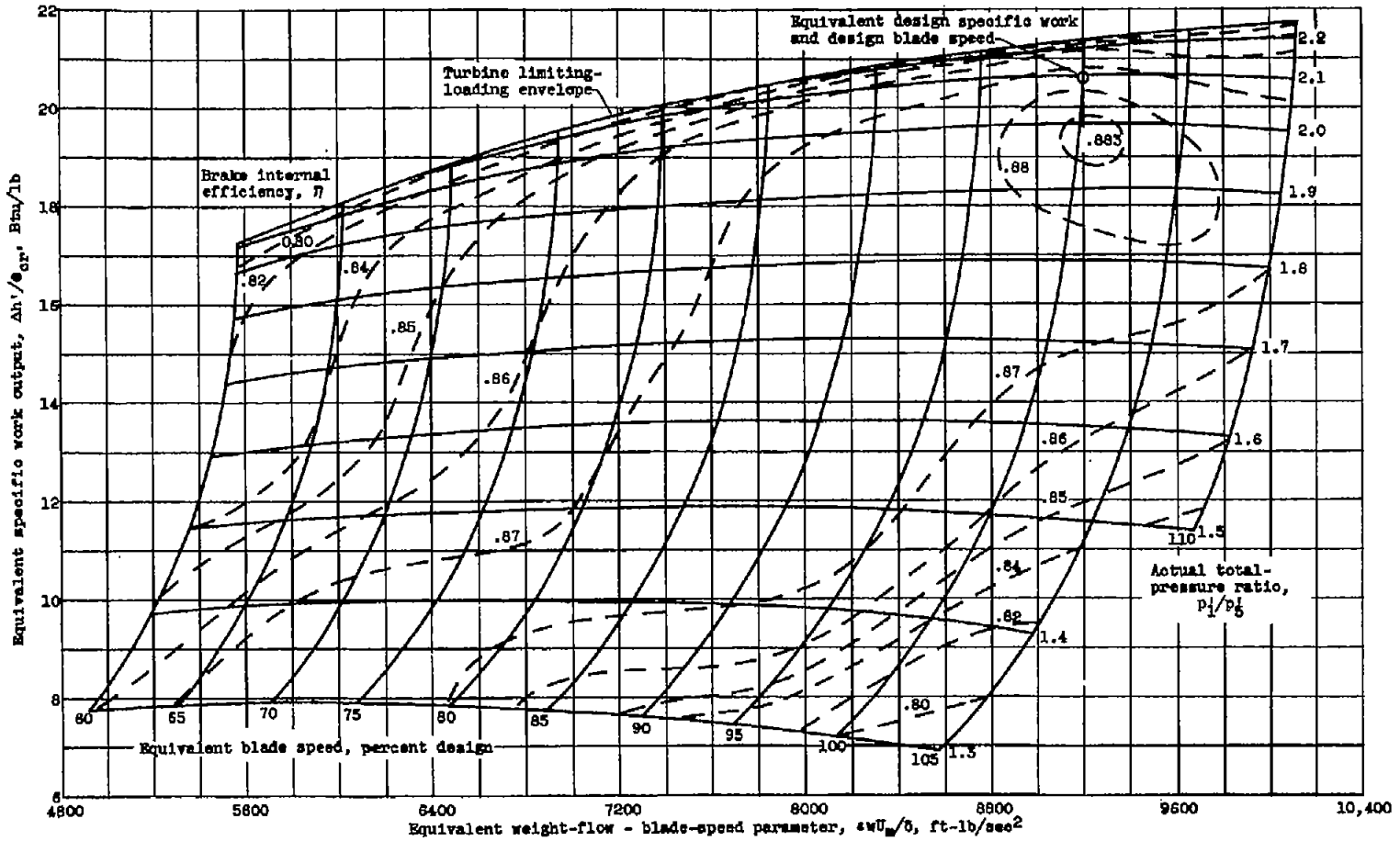
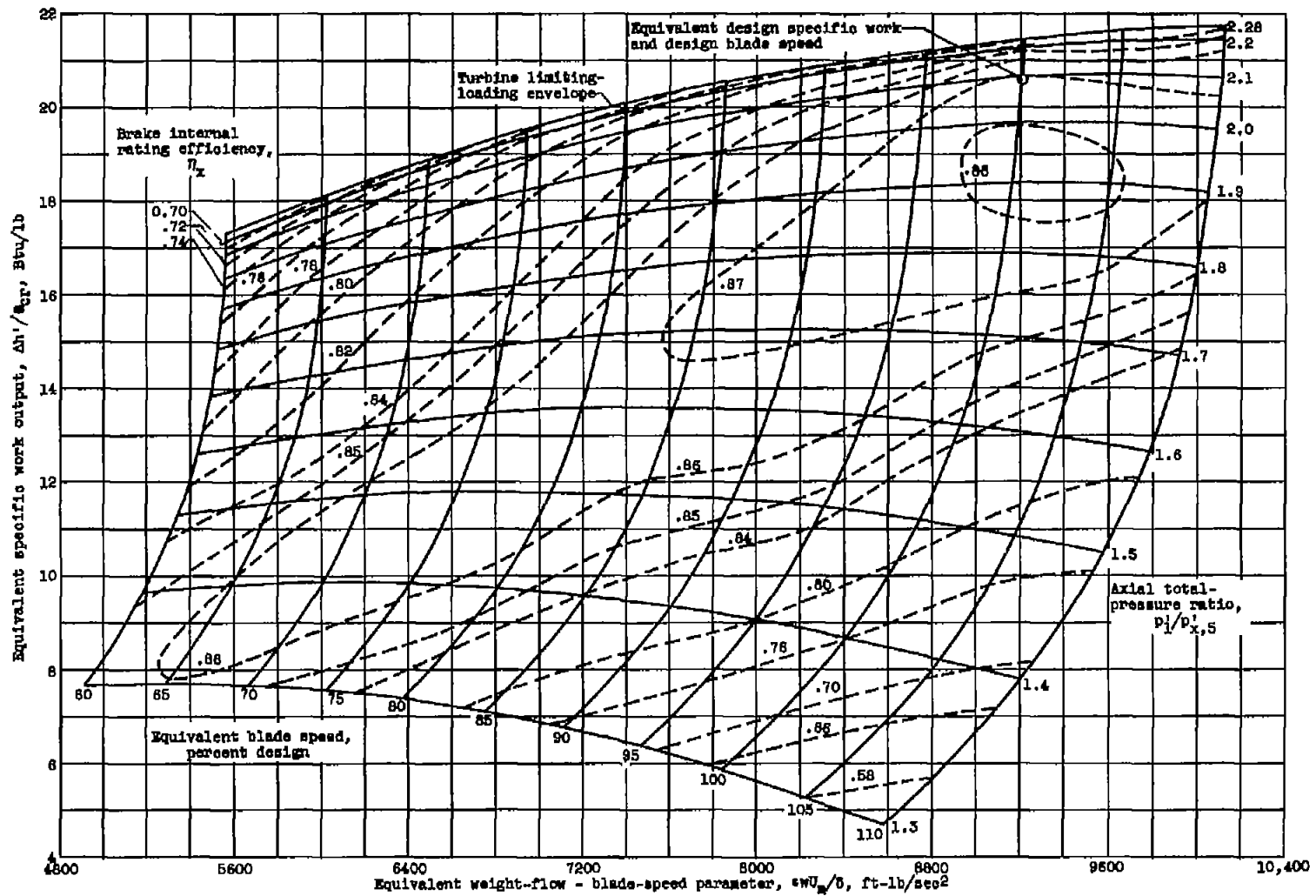


Figure 7. - Schematic section of turbine installation showing instrumentation stations.



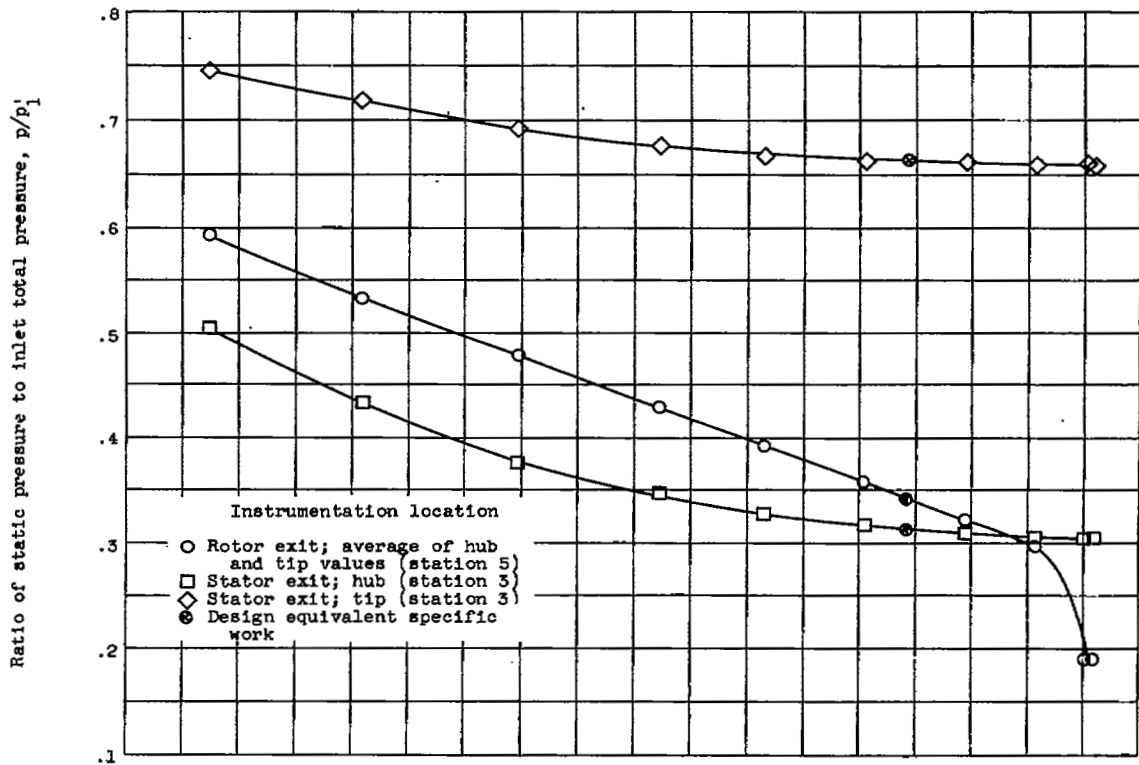
(a) Based on actual total-pressure ratio across turbine.

Figure 8. - Experimentally obtained turbine performance maps.

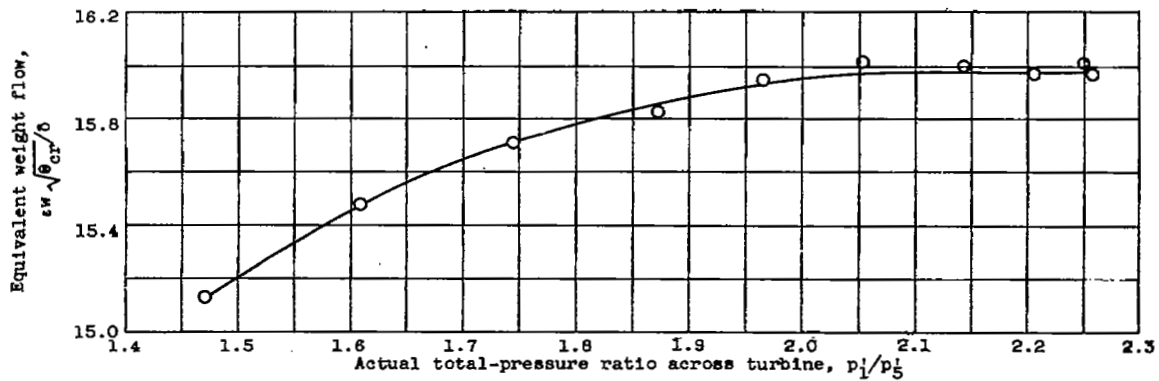


(b) Based on axial total-pressure ratio across turbine.

Figure 8. - Concluded. Experimentally obtained turbine performance maps.



(a) Static pressure behind stator and rotor.



(b) Equivalent weight flow.

Figure 9. - Variation of static pressure behind stator and rotor and equivalent weight flow with actual total-pressure ratio across turbine at design speed.

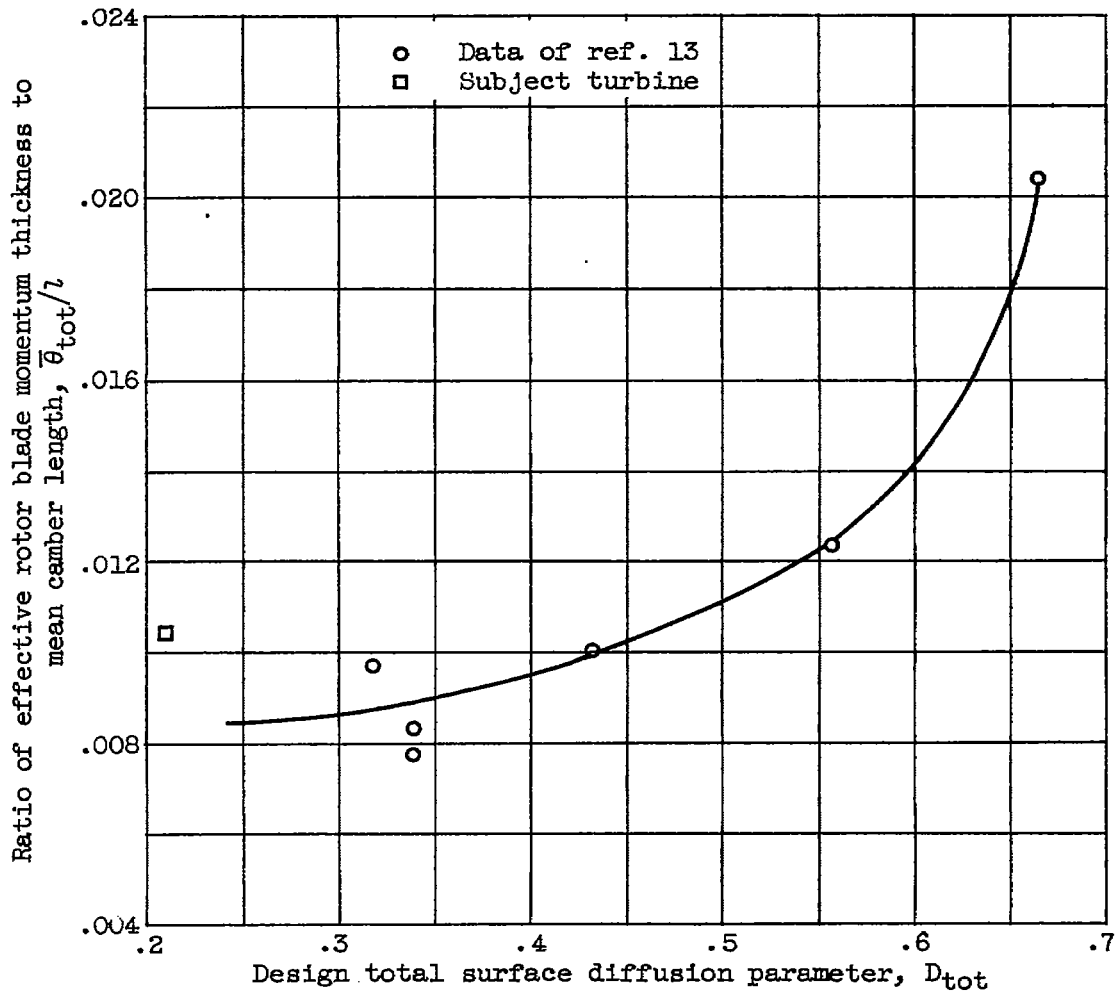


Figure 10. - Comparison of ratio of effective rotor blade momentum thickness to mean camber length of subject turbine with values presented in reference 13.



3 1176 01436 1142

~~CONFIDENTIAL~~